

Pseudogap and preformed pairs in the imbalanced Fermi gas in two dimensions

This article has been downloaded from IOPscience. Please scroll down to see the full text article.

2012 New J. Phys. 14 103044

(<http://iopscience.iop.org/1367-2630/14/10/103044>)

View [the table of contents for this issue](#), or go to the [journal homepage](#) for more

Download details:

IP Address: 146.175.13.243

The article was downloaded on 31/10/2012 at 09:09

Please note that [terms and conditions apply](#).

Pseudogap and preformed pairs in the imbalanced Fermi gas in two dimensions

S N Klimin^{1,3}, J Tempere^{1,2,5} and J T Devreese^{1,4}

¹ Theorie van Kwantumsystemen en Complexe Systemen, Universiteit Antwerpen, Universiteitsplein 1, B-2610 Antwerpen, Belgium

² Lyman Laboratory of Physics, Harvard University, Cambridge, MA 02138, USA

E-mail: jacques.tempere@ua.ac.be

New Journal of Physics **14** (2012) 103044 (22pp)

Received 1 June 2012

Published 29 October 2012

Online at <http://www.njp.org/>

doi:10.1088/1367-2630/14/10/103044

Abstract. The physics of the pseudogap state is intimately linked with the pairing mechanism that gives rise to superfluidity in quantum gases and to superconductivity in high- T_c cuprates, and therefore, both in quantum gases and in superconductors, the pseudogap state and preformed pairs have been under intensive experimental scrutiny. Here, we develop a path integral treatment that provides a divergence-free description of the paired state in two-dimensional Fermi gases. Within this formalism, we derive the pseudogap temperature and the pair fluctuation spectral function, and compare these results with a recent experimental measurement of the pairing in the two-dimensional Fermi gas. The removal of the infrared divergence in the number equations is shown both numerically and analytically, through a study of the long-wavelength and low-energy limit of the pair fluctuation density. Besides the pseudogap temperature, the pair formation temperature and the critical temperature for superfluidity are also derived. The latter corresponds to the Berezinski–Kosterlitz–Thouless (BKT) temperature. The pseudogap temperature, which coincides with the pair formation temperature in the mean field, is found to be suppressed with respect to

³ On leave of absence from Department of Theoretical Physics, State University of Moldova, Strada A Mateevici 60, MD-2009 Kishinev, Republic of Moldova.

⁴ Also at Technische Universiteit Eindhoven, PO Box 513, 5600-MB Eindhoven, The Netherlands.

⁵ Author to whom any correspondence should be addressed.



Content from this work may be used under the terms of the [Creative Commons Attribution-NonCommercial-ShareAlike 3.0 licence](https://creativecommons.org/licenses/by-nc-sa/3.0/). Any further distribution of this work must maintain attribution to the author(s) and the title of the work, journal citation and DOI.

the pair formation temperature by fluctuations. This suppression is strongest for large binding energies of the pairs. Finally, we investigate how the pair formation temperature, the pseudogap temperature and the BKT temperature behave as a function of both binding energy and imbalance between the pairing partners in the Fermi gas. This allows us to set up phase diagrams for the two-dimensional Fermi gas, in which the superfluid phase, the phase-fluctuating quasicondensate and the normal state can be identified.

Contents

1. Introduction	2
2. Thermodynamic functions of the Fermi gas in two dimensions	5
2.1. Gap equation	5
2.2. Gaussian fluctuations	7
2.3. Number equations and the Gaussian pair fluctuation approach	8
2.4. Pair fluctuation spectral functions	9
3. Distribution functions in the long-wavelength limit	11
3.1. Long-wavelength expansion	11
3.2. Structure factor	12
3.3. Distribution functions in the paired state	13
4. Phase diagrams	15
5. Comparison with experiment	17
6. Conclusions	20
Acknowledgments	21
References	21

1. Introduction

Ultracold atomic gases are increasingly used as quantum simulators to probe many-body physics [1]. Recent efforts have focused, in particular, on understanding superfluidity and Cooper pairing in interacting Fermi systems, including *inter alia* the effects of varying the interaction strength, introducing population imbalance and reducing the dimensionality. When these fermionic superfluids are described in the path integral formalism, the thermodynamic potential $\Omega(T, \mu_{\uparrow}, \mu_{\downarrow})$ of the interacting Fermi gas (as a function of temperature T and chemical potentials $\mu_{\uparrow}, \mu_{\downarrow}$ of spin-up and spin-down components) is rewritten as a functional integral over a bosonic field $\Delta_{\mathbf{x},\tau}$ that represents the field of the pairs. This field is introduced through the Hubbard–Stratonovich transformation that allows exact elimination of the fermionic degrees of freedom and results in an action functional for the bosonic field [2]. At first sight, one has only succeeded in rewriting an unsolvable functional integral over fermionic fields by an equally unsolvable functional integral over the bosonic fields. However, the bosonic field lends itself to an obvious simplification when one intuitively feels that a (uniform) Bose–Einstein condensation (BEC) of pairs is present. In that case, one can surmise that $\Delta_{\mathbf{x},\tau} \approx \Delta$, i.e. all pairs are in the zero-momentum state, so the field is a constant in real space. The functional integral can then be replaced by its saddle-point value, substituting $\Delta_{\mathbf{x},\tau} \approx \Delta$ and dropping the integrations. The optimal value of Δ is found by extremizing the action or, equivalently, by minimizing

the thermodynamic potential $\Omega_{\text{sp}}(T, \mu_{\uparrow}, \mu_{\downarrow}; \Delta)$ with respect to the saddle point. When $\Delta = 0$, the (non-interacting) normal Fermi gas is obtained; when $\Delta \neq 0$, the saddle-point approximation bears out a Bose–Einstein condensate of pairs.

In two-dimensional (2D) superfluid systems, the interpretation of the bosonic field is more subtle. To be precise, the condition for BEC has been defined by Penrose and Onsager [5] and Yang [6] as the presence of off-diagonal long-range order, i.e. $\lim_{\mathbf{x} \rightarrow \mathbf{x}'} \langle \Delta_{\mathbf{x}, \tau} \Delta_{\mathbf{x}', \tau} \rangle \neq 0$. At the level of the saddle point, $\Delta_{\mathbf{x}, \tau} \approx \Delta$, it is clear that a non-zero Δ implies BEC. However, as Mermin and Wagner [3] and Hohenberg [4] pointed out, in the 2D system fluctuations play a crucial role: they will prohibit off-diagonal long-range order in uniform systems. These fluctuations around the saddle point are commonly taken into account through the Bogoliubov shift $\Delta_{\mathbf{x}, \tau} = \Delta + \phi_{\mathbf{x}, \tau}$, whereafter $\phi_{\mathbf{x}, \tau}$ is treated as a small fluctuation so that only terms up to second order in $\phi_{\mathbf{x}, \tau}$ are retained in the action functional. Then, for a given Δ , the thermodynamic potential $\Omega(T, \mu_{\uparrow}, \mu_{\downarrow}; \Delta)$ is expressed as a functional integral over the fluctuation fields, with a quadratic action. The quadratic functional integral can be performed, and we obtain a fluctuation correction $\Omega_{\text{fl}}(T, \mu_{\uparrow}, \mu_{\downarrow}; \Delta) = \Omega(T, \mu_{\uparrow}, \mu_{\downarrow}; \Delta) - \Omega_{\text{sp}}(T, \mu_{\uparrow}, \mu_{\downarrow}; \Delta)$ to the thermodynamic potential. The fluctuation fields need not be written down as complex fields $\phi_{\mathbf{x}, \tau}$ resulting from the Bogoliubov shift: equivalent results are obtained by introducing (real) amplitude and phase fluctuation fields through $\Delta_{\mathbf{x}, \tau} \approx \Delta (1 + \delta_{\mathbf{x}, \tau}) e^{i\theta_{\mathbf{x}, \tau}}$.

The culprit suppressing off-diagonal long-range order in 2D is precisely the phase fluctuation field $e^{i\theta_{\mathbf{x}, \tau}}$. Indeed, Mermin and Wagner show that $\langle \Delta_{\mathbf{x}, \tau} \Delta_{\mathbf{x}', \tau} \rangle \approx \langle \Delta^2 e^{i\theta_{\mathbf{x}, \tau}} \rangle \rightarrow 0$ due to the long-wavelength behavior of $\theta_{\mathbf{x}, \tau}$, the relative phase. According to the Penrose–Onsager–Yang criterion, this means that BEC does not occur. However, we can identify other interesting phases from a study of the bosonic pair field $\Delta_{\mathbf{x}, \tau}$. Firstly, $\langle e^{i\theta_{\mathbf{x}, \tau}} \rangle \rightarrow 0$ does not imply that $\Delta = 0$, as noted by Kagan *et al* [7] in their study of quasicondensation. We can identify $\Delta \neq 0$ with the presence of pairing, and search for a transition temperature T_c^* for pair formation separating the $\Delta = 0$ phase from the $\Delta \neq 0$ low-temperature phase. Secondly, although BEC is suppressed, superfluidity can still be present in the 2D system below the Berezinski–Kosterlitz–Thouless [8, 9] (BKT) temperature T_{BKT} . The order parameter for superfluidity is ρ_s , the superfluid density, defined as the phase stiffness and calculated as the prefactor of the $(\nabla \theta_{\mathbf{x}, \tau})^2$ term in the Lagrangian for the phase field, as explained in more detail below. Kosterlitz and Thouless [9] described a mechanism whereby phase stiffness can be lost, namely through the appearance and unbinding of vortex–antivortex pairs that start to proliferate at T_{BKT} and scramble the phase field. This mechanism was observed experimentally in a 2D atomic Bose gas by Dalibard and co-workers [10].

When the bosons under consideration are composite particles, such as Cooper pairs, a third relevant temperature can be identified, related to the density of states of excitations, or equivalently the spectral function for the fluctuations. As we will show below, the fluctuation terms in the density can be expressed through a spectral function $g(\mathbf{q}, \omega)$ describing the contribution of fluctuations with a given wave number \mathbf{q} and momentum ω . In the Nozières and Schmitt-Rink (NSR) formalism [11] for the 2D system [12], the integral over the spectral function is divergent, invalidating the number equations $\partial \Omega / \partial \mu_{\sigma} = n_{\sigma}$, $\sigma = \uparrow, \downarrow$. We show that this divergence is absent when we apply the formalism of Hu *et al* [13–15], which these authors dubbed the Gaussian pair fluctuation (GPF) approach, to the 2D case. As we show below (section 2.3), the GPF approach allows us to set up and simultaneously solve the gap and number equations also in the 2D case. This allows us to derive results for Δ , ρ_s that take into account fluctuations (both phase fluctuations and amplitude fluctuations). The resulting

fluctuation spectra can then be used to obtain the finite-temperature thermodynamics of the 2D Fermi superfluid, following the approach of Salasnich for the three-dimensional (3D) case [16].

In studying the fluctuation spectra, we find that for temperatures above a critical temperature T_p , the fluctuation spectral function $g(\mathbf{q}, \omega)$ becomes negative at long wavelengths ($q < q_c$). This happens at a temperature above T_{BKT} and (obviously) below T_c^* . We interpret this temperature T_p as the pairing temperature at which the pseudogap is open, inspired by recent experiments [17, 18] which investigated pairing in ultracold 2D atomic Fermi gases. For the ultracold atomic gases in 3D, the pseudogap state above the critical temperature is the subject of an intensive study, both experimental and theoretical [19–24], and the similarity with the pseudogap physics in superconductors has not gone unnoticed [25]. In the experiment [17], the spectral function for excitations of the Fermi gas is determined through momentum-resolved photoemission spectroscopy. In [18], the momentum-integrated photoemission spectra are measured, and the evolution of fermion pairing was followed from three to two dimensions by varying the strength of the confining optical lattice. Both experiments reveal a non-zero pairing gap. While the experiments in [17] were interpreted to reveal the pseudogap, i.e. pairing in a non-superfluid state, superfluidity itself has not yet been observed in 2D. Therefore, the existence of the pseudo-gap regime is not experimentally settled until superfluidity itself is observed at temperatures lower than the temperature for pair formation.

We compare the fluctuation spectral functions derived from our microscopic (GPF-based) theory to the measured spectral functions for excitations, and also compare the measured pseudogap temperatures with the calculated T_p as a function of the interaction strength. We find that fluctuations indeed greatly lower the temperature range of existence of the pseudogap phase, especially in the strong-coupling regime. Consequently, in order to obtain a complete phase diagram for the Fermi gas in 2D, we must consider each phase taking into account fluctuations. To the best of our knowledge, this problem has hitherto not been satisfactorily solved for the case of fermions in 2D because of the aforesaid divergence of the density due to fluctuations at finite temperatures. In this paper, as mentioned above, we tackle the problem by correcting the NSR approach using the GPF theory proposed by Hu *et al* [13–15] for the 3D Fermi gas. Moreover, we extend the results to the case of imbalance.

The paper is organized as follows. In section 2, we present the divergence-free method for the self-consistent calculation of thermodynamic parameters of interacting imbalanced fermions in 2D taking into account both amplitude and phase fluctuations. In section 3, density distribution functions for an imbalanced 2D Fermi gas are investigated. In section 4, we discuss finite-temperature phase diagrams for the imbalanced Fermi gas in 2D. In section 5, the theory is applied to the interpretation of the experiment on the pairing of cold atoms in 2D. The discussion is followed by the conclusions in section 6.

Before proceeding with presenting in the next section the functional integral approach in the GPF framework, it is useful to note that the GPF approach we follow here is not the only way to avoid the divergence problem that occurs in the NSR description for the Fermi gas in two dimensions. The NSR scheme and its modifications are related to the T -matrix perturbation approach, in which the effective interaction between pairs is taken into account diagrammatically. In this context, the divergence problem for a Fermi gas in two dimensions can be remedied by taking into account higher orders of the T -matrix expansion—via an effective interaction between pair fluctuations [29]. This interaction stabilizes the superfluid phase of the 2D fermion system at very low temperatures. However, in 2D the T -matrix method does not predict the universal jump in the superfluid density [30] related to the BKT phase transition.

A correct description of the superfluid density becomes possible by explicitly focusing on the phase fluctuations, as in the approach of [26–28, 31]. Within that approach, the bosonic pair field is gauge transformed $\Delta_{\mathbf{x},\tau} e^{i\theta_{\mathbf{x},\tau}}$ and a subsequent gradient expansion of the fluctuation action is performed for phase fluctuations assuming that phase gradients are small. This leads to a quadratic effective action functional of the phase field θ , which, as distinct from the scheme of [11], has no divergence for $\Delta \neq 0$. As far as gradients of the fields are assumed to be small, the resulting effective action is treated as a hydrodynamic action (see, e.g., [32]). The gradient expansion does not contain the *a priori* assumption that fluctuations themselves are small. In this connection, the method was categorized in [26] as non-perturbative. In [33], the present authors applied the method of [26–28, 31] to derive the effective hydrodynamic action for a Fermi gas with a population imbalance. A non-perturbative approach was also the key to develop a description free of infrared and ultraviolet divergences for the 2D Bose gas [34], which successfully describes the crossover between the mean-field regime and the critical fluctuation range corresponding to the BKT transition [35].

2. Thermodynamic functions of the Fermi gas in two dimensions

2.1. Gap equation

We consider a gas of interacting fermions in 2D, with a contact interaction and with s-wave pairing. In the ultracold regime where only s-wave interactions matter, these interactions only take place between ‘spin-up’ and ‘spin-down’ fermions (in practice, these are usually two different hyperfine states of an atomic species). The thermodynamic functions of the Fermi gas are completely determined by the partition function. Here, we will focus on the thermodynamic potential Ω per unit area. The treatment is performed within the path-integral formalism following [33], building on the original path-integral treatment in [2] for the case of a balanced 3D Fermi gas. The partition function is represented as the path integral over Grassmann variables $\bar{\psi}_\sigma(\mathbf{x}, \tau)$, $\psi_\sigma(\mathbf{x}, \tau)$,

$$\mathcal{Z} = e^{-\beta\Omega(T,\mu,\zeta)} = \int \mathcal{D}\psi_{\sigma,\mathbf{x},\tau} \mathcal{D}\bar{\psi}_{\sigma,\mathbf{x},\tau} \exp(-S). \quad (1)$$

The action functional of interacting fermions is given by the integral

$$S = \int_0^\beta d\tau \int d^2\mathbf{x} \sum_{\sigma=\uparrow,\downarrow} \bar{\psi}_{\sigma,\mathbf{x},\tau} \left(\frac{\partial}{\partial\tau} - \nabla_{\mathbf{x}}^2 - \mu_\sigma \right) \psi_{\sigma,\mathbf{x},\tau} + g \int_0^\beta d\tau \int d^2\mathbf{x} \bar{\psi}_{\uparrow,\mathbf{x},\tau} \bar{\psi}_{\downarrow,\mathbf{x},\tau} \psi_{\downarrow,\mathbf{x},\tau} \psi_{\uparrow,\mathbf{x},\tau}, \quad (2)$$

where g is the interaction strength and $\beta = 1/(k_B T)$ is the inverse thermal energy. We choose a system of units where $\hbar = 1$, $2m = 1$ and the Fermi wave vector $k_F \equiv (2\pi n)^{1/2} = 1$ with n the total density. Here, we consider also the case when imbalance is present, i.e. the numbers of spin-up and spin-down atoms are unequal: $n_\uparrow \neq n_\downarrow$. This, in turn, implies that the chemical potentials μ_\uparrow and μ_\downarrow should be fixed separately. Rather than contemplating the separate components, we will work with the total density $n = n_\uparrow + n_\downarrow$ and the density difference $\delta n = n_\uparrow - n_\downarrow$. Correspondingly, we will use the average chemical potential $\mu = (\mu_\uparrow + \mu_\downarrow)/2$ and the chemical potential difference $\zeta = (\mu_\uparrow - \mu_\downarrow)/2$. Note that the total density is equal to $1/(2\pi)$ in our units, so this means that we need to solve the number equation to fix μ (in the non-interacting case, $\mu = 1$ in our units). Only with respect to the imbalance, we have a choice of studying the free

energy (and making phase diagrams as a function of δn) or the thermodynamic potential Ω (and making phase diagrams as a function of ζ). The thermodynamic potential is linked to the free energy by the usual Legendre transform and, as mentioned, in our formalism this corresponds to imposing the number equations.

The strength g of the contact interaction is renormalized as in [36, 37] using the binding energy E_b for a two-particle bound state, which always exists in 2D [43, 44]:

$$\frac{1}{g} = \frac{1}{8\pi} \left(\ln \frac{E_b}{E} + i\pi \right) - \int \frac{d^2\mathbf{k}}{(2\pi)^2} \frac{1}{2k^2 - E + i\delta}, \quad (3)$$

with δ a positive infinitesimal number. The BCS regime corresponds to $E_b/E_F \ll 1$, whereas the BEC regime corresponds to the opposite ratio $E_b/E_F \gg 1$. Similarly to [2], we introduce the pair field $\Delta_{\mathbf{x},\tau}$ and perform the Hubbard–Stratonovich transformation, which results in a fermion–boson action quadratic in fermion variables. After integrating out the fermion variables, the following effective bosonic action is obtained as a function of the Hubbard–Stratonovich pair field $\Delta_{\mathbf{x},\tau}$:

$$S_{\text{eff}} = -\text{tr} [\ln (-\mathbb{G}^{-1})] - \int_0^\beta d\tau \int d^2\mathbf{x} \frac{\bar{\Delta}_{\mathbf{x},\tau} \Delta_{\mathbf{x},\tau}}{g}, \quad (4)$$

where \mathbb{G}^{-1} is the inverse of the Nambu propagator

$$-\mathbb{G}^{-1} = \sigma_0 \left(\frac{\partial}{\partial \tau} - \zeta \right) - \sigma_3 (\nabla^2 + \mu) - \sigma_1 \Delta_{\mathbf{x},\tau}. \quad (5)$$

Here, σ_j are the Pauli matrices. As far as the effective action S_{eff} is not a quadratic functional of the Hubbard–Stratonovich pair field, the resulting functional integral over the pair field

$$\mathcal{Z} \propto \int \mathcal{D}\Delta_{\mathbf{x},\tau} \mathcal{D}\bar{\Delta}_{\mathbf{x},\tau} \exp(-S_{\text{eff}}) \quad (6)$$

cannot be calculated analytically exactly. As in the analogous problem in 3D [2, 38, 39], and as explained in the introduction, we consider approximations provided by an expansion of the effective action S_{eff} over fluctuations of the pair field $\Delta_{\mathbf{x},\tau}$ about its saddle-point value Δ . The phase diagrams of a 2D Fermi gas in the saddle-point approximation have been investigated in [37, 40]. The effective saddle-point action provides the thermodynamic potential per unit area:

$$\Omega_{\text{sp}}(T, \mu, \zeta; \Delta) = - \int \frac{d^2\mathbf{k}}{(2\pi)^2} \left[\frac{\ln(2 \cosh \beta E_{\mathbf{k}} + 2 \cosh \beta \zeta)}{\beta} - \xi_{\mathbf{k}} \right] - \frac{\Delta^2}{g}. \quad (7)$$

Here, $\xi_{\mathbf{k}} = k^2 - \mu$ is the fermion energy and $E_{\mathbf{k}} = \sqrt{\xi_{\mathbf{k}}^2 + \Delta^2}$ is the Bogoliubov excitation energy. The gap parameter Δ is determined from the gap equation generalized to the imbalance case—the minimum condition for the saddle-point thermodynamic potential as a function of the gap parameter Δ at fixed temperature and chemical potentials:

$$\frac{\partial \Omega_{\text{sp}}(\beta, \mu, \zeta; \Delta)}{\partial \Delta} = 0. \quad (8)$$

For high temperatures ($T > T_c^*$) or at high levels of imbalance ($\zeta > \zeta_c$), the thermodynamic potential will have its minimum at $\Delta = 0$, the unpaired normal state. Following the experimental observation of superfluidity in imbalanced Fermi gases in 3D [41], the phase diagram of the

imbalanced Fermi gas has attracted much attention (for a recent review, see [42]). To find the phase diagrams in 2D, the above gap equation has to be solved in conjunction with the number equations discussed in the remainder of this section.

2.2. Gaussian fluctuations

The next-order approximation brings into account fluctuations about the saddle point:

$$\begin{cases} \Delta_{\mathbf{x},\tau} = \Delta + \phi_{\mathbf{x},\tau}, \\ \bar{\Delta}_{\mathbf{x},\tau} = \Delta + \bar{\phi}_{\mathbf{x},\tau}. \end{cases}$$

We apply the Fourier expansion of the fluctuation coordinates:

$$\phi_{\mathbf{x},\tau} = \frac{1}{L\sqrt{\beta}} \sum_{\mathbf{q}} \sum_{n=-\infty}^{\infty} e^{i\mathbf{q}\cdot\mathbf{r}-i\omega_n\tau} \varphi_{\mathbf{q}}(\omega_n), \quad (9)$$

$$\bar{\phi}_{\mathbf{x},\tau} = \frac{1}{L\sqrt{\beta}} \sum_{\mathbf{q}} \sum_{n=-\infty}^{\infty} e^{-i\mathbf{q}\cdot\mathbf{r}+i\omega_n\tau} \bar{\varphi}_{\mathbf{q}}(\omega_n), \quad (10)$$

where L is the linear size of the 2D system and $\omega_n = 2\pi n/\beta$ (with $n = 0, \pm 1, \pm 2, \dots$) are the bosonic Matsubara frequencies. The quadratic fluctuation contribution to the effective bosonic action is the functional of complex fluctuation coordinates similar to that derived in [39]:

$$S_{\text{fl}} = \sum_{\mathbf{q}} \sum_{n=-\infty}^{\infty} \left\{ M_{1,1}(\mathbf{q}, i\omega_n) \bar{\varphi}_{\mathbf{q}}(\omega_n) \varphi_{\mathbf{q}}(\omega_n) + \frac{1}{2} M_{1,2}(\mathbf{q}, i\omega_n) [\bar{\varphi}_{\mathbf{q}}(\omega_n) \bar{\varphi}_{-\mathbf{q}}(\omega_{-n}) + \varphi_{\mathbf{q}}(\omega_n) \varphi_{-\mathbf{q}}(\omega_{-n})] \right\}, \quad (11)$$

where $M_{j,k}(\mathbf{q}, i\omega_n)$ are the matrix elements of the inverse pair fluctuation propagator. They are determined by the expressions (cf [39])

$$M_{1,1}(\mathbf{q}, i\omega_n) = -\frac{1}{g} + \int \frac{d^2\mathbf{k}}{(2\pi)^2} \frac{X(E_{\mathbf{k}})}{2E_{\mathbf{k}}} \left(\frac{(i\omega_n - E_{\mathbf{k}} + \xi_{\mathbf{k}+\mathbf{q}})(E_{\mathbf{k}} + \xi_{\mathbf{k}})}{(i\omega_n - E_{\mathbf{k}} + E_{\mathbf{k}+\mathbf{q}})(i\omega_n - E_{\mathbf{k}} - E_{\mathbf{k}+\mathbf{q}})} - \frac{(i\omega_n + E_{\mathbf{k}} + \xi_{\mathbf{k}+\mathbf{q}})(E_{\mathbf{k}} - \xi_{\mathbf{k}})}{(i\omega_n + E_{\mathbf{k}} - E_{\mathbf{k}+\mathbf{q}})(i\omega_n + E_{\mathbf{k}} + E_{\mathbf{k}+\mathbf{q}})} \right) \quad (12)$$

and

$$M_{1,2}(\mathbf{q}, i\omega_n) = -\Delta^2 \int \frac{d^2\mathbf{k}}{(2\pi)^2} \frac{X(E_{\mathbf{k}})}{2E_{\mathbf{k}}} \left(\frac{1}{(i\omega_n - E_{\mathbf{k}} + E_{\mathbf{k}+\mathbf{q}})(i\omega_n - E_{\mathbf{k}} - E_{\mathbf{k}+\mathbf{q}})} + \frac{1}{(i\omega_n + E_{\mathbf{k}} - E_{\mathbf{k}+\mathbf{q}})(i\omega_n + E_{\mathbf{k}} + E_{\mathbf{k}+\mathbf{q}})} \right). \quad (13)$$

Here, the following function has been introduced:

$$X(E_{\mathbf{k}}) = \frac{\sinh(\beta E_{\mathbf{k}})}{\cosh(\beta E_{\mathbf{k}}) + \cosh(\beta \zeta)}. \quad (14)$$

The integration over fluctuation coordinates gives us the fluctuation contribution $\Omega_{\text{fl}}(T, \mu, \zeta; \Delta)$ to the total grand-canonical thermodynamic potential Ω per unit area:

$$\Omega_{\text{fl}}(T, \mu, \zeta; \Delta) = \frac{1}{2\beta} \int \frac{d^2\mathbf{q}}{(2\pi)^2} \sum_{n=-\infty}^{\infty} \ln [\Gamma(\mathbf{q}, i\omega_n)] \quad (15)$$

with

$$\Gamma(\mathbf{q}, i\omega_n) = M_{1,1}(\mathbf{q}, i\omega_n)M_{1,1}(\mathbf{q}, -i\omega_n) - M_{1,2}(\mathbf{q}, i\omega_n)M_{1,2}(\mathbf{q}, -i\omega_n). \quad (16)$$

2.3. Number equations and the Gaussian pair fluctuation approach

The fermion density and the density difference fix the chemical potentials μ and ζ through the derivatives of the total thermodynamic potential per unit area:

$$n = - \left. \frac{\partial \Omega}{\partial \mu} \right|_{T, \zeta}, \quad (17)$$

$$\delta n = - \left. \frac{\partial \Omega}{\partial \zeta} \right|_{T, \mu} \quad (18)$$

(note that in our units $n = 1/2\pi$). We can write out these equations by splitting the total thermodynamic potential into saddle point and fluctuation contributions:

$$n = - \left. \frac{\partial \Omega_{\text{sp}}}{\partial \mu} \right|_{T, \zeta} - \left. \frac{\partial \Omega_{\text{fl}}}{\partial \mu} \right|_{T, \zeta}, \quad (19)$$

$$\delta n = - \left. \frac{\partial \Omega_{\text{sp}}}{\partial \zeta} \right|_{T, \mu} - \left. \frac{\partial \Omega_{\text{fl}}}{\partial \zeta} \right|_{T, \mu}. \quad (20)$$

We will denote the first and second terms on the right-hand side (rhs) of expression (19) for n by n_{sp} and n_{fl} , respectively. Similarly, the terms on the rhs of expression (20) will be denoted by δn_{sp} and δn_{fl} . Note that the thermodynamic potentials obtained from expressions (7) and (15) are expressed as a function not only of T, μ, ζ , but also of Δ . This gap Δ is not an independent thermodynamic variable, and when considering $\Omega(T, \mu, \zeta, \Delta)$ explicitly as a function of also Δ , the implicit dependence of Δ on the chemical potentials must be taken into account in (19), (20):

$$n = - \left. \frac{\partial \Omega_{\text{sp}}}{\partial \mu} \right|_{T, \zeta, \Delta} - \left. \frac{\partial \Omega_{\text{fl}}}{\partial \mu} \right|_{T, \zeta, \Delta} - \left. \frac{\partial \Omega_{\text{fl}}}{\partial \Delta} \right|_{T, \zeta, \mu} \left. \frac{\partial \Delta}{\partial \mu} \right|_{T, \zeta}, \quad (21)$$

$$\delta n = - \left. \frac{\partial \Omega_{\text{sp}}}{\partial \zeta} \right|_{T, \mu, \Delta} - \left. \frac{\partial \Omega_{\text{fl}}}{\partial \zeta} \right|_{T, \mu, \Delta} - \left. \frac{\partial \Omega_{\text{fl}}}{\partial \Delta} \right|_{T, \zeta, \mu} \left. \frac{\partial \Delta}{\partial \zeta} \right|_{T, \mu}.$$

Note that the gap equation $\partial \Omega_{\text{sp}} / \partial \Delta = 0$ at fixed T, μ, ζ implies that the implicit dependence of Δ on the chemical potentials will only affect the fluctuation part of the thermodynamic potential in the above equations. Different theories of the BEC–BCS crossover, in any dimension, can be categorized by their choice of number and gap equations. The simplest mean field approach only keeps the terms with Ω_{sp} . The Nozières and Schmitt-Rink approach includes the second terms in the rhs of expressions (21). Finally, the GPF approach includes the last term on the rhs of expressions (21). Note that in the literature, there is no common opinion on which approach

is the best. For example, on the one hand, Randeria *et al* [45, 46], Hu *et al* [13] and Keeling *et al* [47] state that the derivative over μ must be performed taking into account a variation of the gap determined by the gap equation. On the other hand, Ohashi *et al* [48–50] and Strinati *et al* [51, 52] use the other definition, considering Δ in the number equations as an independent variable and, therefore, applying the gap equation *after* taking the derivatives $\partial\Omega/\partial\mu$. In the papers [48–50], it is stated that the last terms in (21) are the higher-order corrections with respect to Gaussian quadratic fluctuations. Keeling *et al* [47] correctly argue that both terms in those derivatives are of one and the same order and emphasize that the existence of the second term is crucial in two dimensions. Below, we demonstrate the key significance of taking into account the last terms in (21) for the convergence of fluctuation contributions to the fermion density in 2D.

As stated in the introduction, in order to treat the fluctuations, there is an alternative to the Bogoliubov shift $\Delta_{\mathbf{x},\tau} = \Delta + \phi_{\mathbf{x},\tau}$, namely the parametrization in amplitude and phase fluctuations $\Delta_{\mathbf{x},\tau} \approx \Delta(1 + \delta_{\mathbf{x},\tau})e^{i\theta_{\mathbf{x},\tau}}$. When, *after* this parametrization, the effective action is expanded with respect to $\delta_{\mathbf{x},\tau}$ and $\theta_{\mathbf{x},\tau}$ (rather than $\phi_{\mathbf{x},\tau}$ and $\bar{\phi}_{\mathbf{x},\tau}$), this leads to another quadratic fluctuation action S'_{fl} which differs from expression (11) for S_{fl} only by terms that vanish when applying the gap equation. Correspondingly, the thermodynamic potentials Ω_{fl} and Ω'_{fl} provided by those two actions lead to one and the same contribution to the fermion density. Furthermore, keeping in S'_{fl} only the leading order long-wavelength and low-energy terms leads to the same effective ‘hydrodynamic’ action as in [33]. In the particular case of a balanced gas, the effective action of [33] turns into the result of [26, 31]. This means that the effective action described as the result of the non-perturbative approach in [26] can be equivalently re-derived within the perturbative NSR-like scheme. Moreover, the present treatment can be considered as an extension of the approach of [26, 31, 33] beyond the long-wavelength and low-energy approximation (and to imbalanced 2D gases). The hydrodynamic action is particularly useful in extracting the superfluid density ρ_s , by identifying it with the prefactor of the $(\nabla\theta_{\mathbf{x},\tau})^2/2$ term in the expression for S'_{fl} . This identification yields straightforwardly [33]

$$\rho_s(T, \mu, \zeta, \Delta) = \frac{1}{4\pi} \int_0^\infty dk k \left(1 - \frac{\xi_k}{E_k} X(E_k) - k^2 X'(E_k) \right) \quad (22)$$

with $X(E_k)$ given by expression (14) and $X'(E_k)$ its first derivative, evaluated in E_k . Once Δ , μ , ζ are obtained for a given temperature (and interaction strength) by solving the gap and number equations, they can be substituted in this expression to determine whether the system is in the superfluid phase ($\rho_s \neq 0$) or the normal phase ($\rho_s = 0$). As discussed in the results section, we also use this expression to find the temperature T_{BKT} of the phase transition between those two states. Already we note that $\Delta = 0$ leads to $\rho_s = 0$, so that $T_{\text{BKT}} < T_c^*$ and the superfluid state requires pair formation, as it should.

2.4. Pair fluctuation spectral functions

From expression (7) for the saddle-point thermodynamic potential, we derive the following expressions for the saddle-point densities:

$$n_{\text{sp}} := - \left. \frac{\partial\Omega_{\text{sp}}}{\partial\mu} \right|_{T,\zeta,\Delta} = \int \frac{d^2\mathbf{k}}{(2\pi)^2} \left(1 - \frac{\xi_{\mathbf{k}}}{E_{\mathbf{k}}} \frac{\sinh(\beta E_{\mathbf{k}})}{\cosh(\beta\zeta) + \cosh(\beta E_{\mathbf{k}})} \right), \quad (23)$$

$$\delta n_{\text{sp}} := - \left. \frac{\partial\Omega_{\text{sp}}}{\partial\zeta} \right|_{T,\zeta} = \int \frac{d^2\mathbf{k}}{(2\pi)^2} \frac{\sinh(\beta\zeta)}{\cosh(\beta\zeta) + \cosh(\beta E_{\mathbf{k}})}. \quad (24)$$

Similarly, the fluctuation contributions to the fermion densities are determined using (15) and using the GPF approach. The results can be written as a sum over wavelengths and frequencies of pair fluctuation structure factors:

$$n_{\text{fl}} := - \left. \frac{\partial \Omega_{\text{fl}}}{\partial \mu} \right|_{T, \zeta} = - \int \frac{d^2 \mathbf{q}}{(2\pi)^2} \frac{1}{\beta} \sum_{n=-\infty}^{\infty} J(\mathbf{q}, i\omega_n), \quad (25)$$

$$\delta n_{\text{fl}} := - \left. \frac{\partial \Omega_{\text{fl}}}{\partial \zeta} \right|_{T, \mu} = - \int \frac{d^2 \mathbf{q}}{(2\pi)^2} \frac{1}{\beta} \sum_{n=-\infty}^{\infty} K(\mathbf{q}, i\omega_n). \quad (26)$$

The pair fluctuation structure factors J and K are given by

$$J(\mathbf{q}, i\omega_n) = \frac{1}{\Gamma(\mathbf{q}, i\omega_n)} \left[\frac{\partial M_{1,1}(\mathbf{q}, i\omega_n)}{\partial \mu} M_{1,1}(\mathbf{q}, -i\omega_n) - \frac{\partial M_{1,2}(\mathbf{q}, i\omega_n)}{\partial \mu} M_{1,2}(\mathbf{q}, -i\omega_n) \right], \quad (27)$$

$$K(\mathbf{q}, i\omega_n) = \frac{1}{\Gamma(\mathbf{q}, i\omega_n)} \left[\frac{\partial M_{1,1}(\mathbf{q}, i\omega_n)}{\partial \zeta} M_{1,1}(\mathbf{q}, -i\omega_n) - \frac{\partial M_{1,2}(\mathbf{q}, i\omega_n)}{\partial \zeta} M_{1,2}(\mathbf{q}, -i\omega_n) \right]. \quad (28)$$

We transform the Matsubara summations in (25) and (26) into the contour integrals in the complex plane as follows:

$$\frac{1}{\beta} \sum_{n=-\infty}^{\infty} J(\mathbf{q}, i\omega_n) = \frac{1}{\pi} \int_{-\infty}^{\infty} \frac{\text{Im} J(\mathbf{q}, \omega + i\delta)}{e^{\beta\omega} - 1} d\omega, \quad \delta \rightarrow +0. \quad (29)$$

This allows us to express the resulting fluctuation contributions to the fermion density through the distribution functions for pair excitations:

$$n_{\text{fl}} = \frac{1}{2\pi^2} \int_0^{\infty} g_n(q) q dq, \quad (30)$$

$$\delta n_{\text{fl}} = \frac{1}{2\pi^2} \int_0^{\infty} g_{\delta n}(q) q dq. \quad (31)$$

The fluctuation distribution functions $g_n(q)$ and $g_{\delta n}(q)$ are the integrals over the frequency with the pair fluctuation structure factors:

$$g_n(q) = - \int_{-\infty}^{\infty} \frac{\text{Im} J(q, \omega + i\delta)}{e^{\beta\omega} - 1} d\omega, \quad (32)$$

$$g_{\delta n}(q) = - \int_{-\infty}^{\infty} \frac{\text{Im} K(q, \omega + i\delta)}{e^{\beta\omega} - 1} d\omega. \quad (33)$$

The functions $g_n(q)$ and $g_{\delta n}(q)$ are proportional to the densities of states for the pair fluctuations. The behavior of these functions is crucial for understanding the pseudogap properties and the different phase transitions in the imbalanced 2D Fermi gas. In the NSR approach, the fluctuation distribution functions have a divergence, and as a consequence no value of the chemical potential μ can be found so that the number equation $n_{\text{sp}} + n_{\text{fl}} = n = 1/(2\pi)$ is satisfied. In the GPF approach, the divergence is overcome and the number equation can be satisfied. In order to demonstrate this, we focus in the next section on the long-wavelength limit where exact analytic expressions for the distribution functions are obtained.

3. Distribution functions in the long-wavelength limit

3.1. Long-wavelength expansion

In order to investigate the problem of the long-wavelength convergence for the fluctuation contributions to the density, it is necessary to derive analytically the spectrum of low-lying and long-wavelength pair excitations. For this purpose, we expand the matrix elements of the inverse pair fluctuation propagator $M_{j,k}(q, z)$ in powers of (q, z) up to the second-order terms in power of z and q ,

$$M_{1,1}(\mathbf{q}, z) \approx A + Bq^2 + Cz + Fz^2, \quad (34)$$

$$M_{1,2}(\mathbf{q}, z) \approx D + Eq^2 + Hz^2. \quad (35)$$

The derivation of the coefficients is rather tedious. In this connection, only the final results are presented here. The coefficients in the $M_{1,1}$ expansion are given by

$$A = \frac{1}{2\pi} \int_0^\infty k dk \left(\frac{1}{2k^2 - E_b} - \frac{E_k^2 + \xi_k^2}{4E_k^3} X(E_k) - \frac{\Delta^2}{4} \frac{X'(E_k)}{E_k^2} \right), \quad (36)$$

$$B = \frac{1}{16\pi} \int_0^\infty k dk \frac{k^2 (E_k^4 + 7E_k^2 \xi_k^2 - 10\xi_k^4) - E_k^4 \xi_k + 3\xi_k^3 E_k^2}{E_k^7} X(E_k) \\ + \frac{\Delta^2}{8\pi} \int_0^\infty k dk \left(\frac{\xi_k (E_k^2 - 3k^2 \xi_k)}{E_k^6} X'(E_k) \right. \\ \left. + \frac{\xi_k (3k^2 \xi_k - E_k^2) - k^2 E_k^2}{2E_k^5} X''(E_k) - \frac{k^2 \xi_k^2}{3E_k^4} X^{(3)}(E_k) \right), \quad (37)$$

$$C = -\frac{1}{8\pi} \int_0^\infty k dk \frac{\xi_k}{E_k^3} X(E_k) - \frac{\Delta^2}{8\pi} \int_0^\infty k dk \frac{X'(E_k)}{\xi_k E_k^2}, \quad (38)$$

$$F = -\frac{1}{32\pi} \int k dk \frac{E_k^2 + \xi_k^2}{E_k^5} X(E_k) \quad (39)$$

and those in the $M_{1,2}$ expansion are given by

$$D = \frac{\Delta^2}{8\pi} \int_0^\infty k dk \frac{X(E_k) - E_k X'(E_k)}{E_k^3}, \quad (40)$$

$$E = \frac{\Delta^2}{16\pi} \int_0^\infty k dk \frac{10k^2 \xi_k^2 - 3E_k^2 (\xi_k + k^2)}{E_k^7} X(E_k) + \frac{\Delta^2}{8\pi} \int_0^\infty k dk \left(\frac{\xi_k E_k^2 + k^2 E_k^2 - 3k^2 \xi_k^2}{2E_k^6} \right. \\ \left. \times [2X'(E_k) - E_k X''(E_k)] - \frac{\xi_k^2 k^2}{3E_k^4} X^{(3)}(E_k) \right), \quad (41)$$

$$H = \frac{\Delta^2}{32\pi} \int_0^\infty k dk \frac{X(E_k)}{E_k^5}.$$

In these expressions X' , X'' and $X^{(3)}$ are the first, second and third derivatives of the function X given by expression (14), with respect to its argument. In the literature, an analogous expansion was performed for 3D at finite temperatures in [48–50] in the strong-coupling limit, and in [45] at low temperatures. The present expansion is all-coupling and all-temperature, because no restriction is imposed on the thermodynamic parameters.

3.2. Structure factor

Let us substitute the expansions (34) and (35) into the structure factor $J(\mathbf{q}, z)$ in order to obtain its long-wavelength and low-energy form $J_{\text{lw}}(\mathbf{q}, z)$. The spectrum of pair bosonic excitations is determined by the poles of $J_{\text{lw}}(\mathbf{q}, z)$. In the long-wavelength and low-energy range, these roots are $z = \pm\omega_q$ with the pair excitation frequency ω_q which satisfies the Goldstone theorem

$$\omega_q = q\sqrt{v^2 + \kappa^2 q^2} \quad (42)$$

with the parameters (cf the analogous expansion in the 3D case [53])

$$v = \sqrt{\frac{2A(B-E)}{C^2 + 2A(H-F)}}, \quad (43)$$

$$\kappa = \sqrt{\frac{C^2(B-E)(4A(BH-EF) + C^2(B+E))}{(C^2 + 2A(H-F))^3}}. \quad (44)$$

The parameter v has the dimensionality of velocity and tends to the first sound velocity in the low-temperature limit. As far as the parameter D is proportional to Δ^2 , the velocity parameter for pair excitations tends to zero at the phase boundary when $\Delta = 0$. In the BEC limit, when $E_b \gg 1$, we find that $\mu \rightarrow -E_b/2$ and $\kappa \rightarrow 1/4$. This results in the pair excitation spectrum $\omega_q \rightarrow q^2/2$ at the BEC side.

In order to calculate the long-wavelength distribution function, we keep the lowest-order terms in powers of z and q^2 in the numerator of $J_{\text{lw}}(\mathbf{q}, z)$. This gives us the result

$$J_{\text{lw}}(\mathbf{q}, z) = \frac{a_q}{z - \omega_q} + \frac{b_q}{z + \omega_q}, \quad (45)$$

where the coefficients a_q and b_q are related to the constants determined above as

$$a_q = \frac{\alpha + \lambda\omega_q + \chi q^2}{2\omega_q [C^2 + 2A(H-F)]}, \quad b_q = -\frac{\alpha - \lambda\omega_q + \chi q^2}{2\omega_q [C^2 + 2A(H-F)]} \quad (46)$$

with the notations

$$\alpha = D_\mu D - A_\mu A, \quad \lambda = A_\mu C - C_\mu A, \quad \chi = E_\mu D + D_\mu E - A_\mu B - B_\mu A. \quad (47)$$

Here A_μ, B_μ, \dots are the derivatives $A_\mu \equiv \partial A / \partial \mu$, etc. The distribution function is calculated by setting $z = \omega + i\delta$ with $\delta \rightarrow +0$. This gives us the structure factor as a superposition of the delta functions. The distribution function then takes the form

$$g_n^{(\text{lw})}(q) = \frac{1}{4\pi} \frac{\lambda}{C^2 + 2A(H-F)} \left[\frac{\alpha + \chi q^2}{\lambda\omega_q} \coth\left(\frac{\beta\omega_q}{2}\right) - 1 \right]. \quad (48)$$

For the other distribution function $g_{\delta n}^{(\text{lw})}(q)$, the derivations are the same, but with a replacement of the derivatives over μ by the corresponding derivatives over ζ .

3.3. Distribution functions in the paired state

Here we consider the paired state of the quasicondensate in which the gap parameter $\Delta \neq 0$. In this case, the gap parameter obeys the gap equation

$$\frac{1}{4\pi} \int_0^\infty \frac{X(E_{\mathbf{k}})}{E_{\mathbf{k}}} k \, dk + \frac{1}{g} = 0. \quad (49)$$

The strength g of the contact interaction is expressed through the two-particle binding energy E_b in 2D by equation (3). The difference of coefficients $A - D$ is proportional to the left-hand side (lhs) of the gap equation. Therefore, as long as the gap equation is satisfied, we obtain $D = A$. Moreover, because the derivatives of matrix elements are calculated while keeping the gap equation satisfied, we find that $A_\mu = D_\mu$ and $A_\zeta = D_\zeta$. This implies, in particular, that the coefficient $\alpha = 0$, as is evident from expression (47), and we find that

$$g_n^{(lw)}(q) = \frac{1}{4\pi} \frac{\lambda}{C^2 + 2A(H - F)} \left[\frac{\chi q^2}{\lambda \omega_q} \coth\left(\frac{\beta\omega_q}{2}\right) - 1 \right]. \quad (50)$$

Thus $g_n^{(lw)}(q)$ tends to a finite value at $q \rightarrow 0$ for $\Delta \neq 0$, and behaves as q^{-2} at $q \rightarrow 0$ for $\Delta = 0$. As a result, the fluctuation contributions n_{fl} and δn_{fl} in 2D are *finite* at $\Delta \neq 0$. They can diverge only at $\Delta = 0$. This is to be contrasted with the NSR scheme, where the order parameter Δ is treated as an independent variable and where n_{fl} and δn_{fl} in 2D diverge *for all* Δ .

Figure 1 shows the behavior of the fluctuation distribution functions $g_n(q)$ and $g_{\delta n}(q)$ for different temperatures, at binding energy $E_b = 0.5$ and at the critical value of the chemical potential imbalance $\zeta = \zeta_c(E_b, T)$. The critical value ζ_c for a given (E_b, T) is determined as the highest imbalance at which the order parameter Δ is other than zero. The dashed lines correspond to the NSR scheme and reveal a q^{-2} long-wavelength divergence. The full lines show the results in the GPF scheme, where the long-wavelength divergence is absent. This behavior is seen for both $g_n(q)$ and $g_{\delta n}(q)$. In the limit $\Delta \rightarrow 0$, the functions $qg_n(q)$ and $qg_{\delta n}(q)$ become logarithmically divergent. However, the sign of this divergence is *opposite* of that of the divergence of the functions calculated neglecting the variation of Δ .

For the lower temperature shown in figure 1, $T/T_F = 0.1$, $g_n(q)$ remains positive, whereas for the higher temperature $T/T_F = 0.3$, there is a sign change in $g_n(q)$ as it becomes negative for small q . Regions of negative value for the fluctuation distribution function $g_{\delta n}(q)$ are expected, as the sign will change depending on which species is the majority species. However, $g_n(q)$ is expected to remain positive, as it is proportional to the pair fluctuation density of states. The appearance of a long-wavelength instability heralds the breakdown of the paired state. We can track the onset of this instability by studying $g_n(q \rightarrow 0)$ as a function of temperature. At low temperatures, $g_n(0)$ is positive, and the fluctuation density function remains positive for all q . At high temperatures $g_n(0)$ becomes negative, signalling the long-wavelength instability. We denote the temperature separating the two regions by T_p , and find this temperature through solving $g_n(0) = 0$ with respect to temperature. The behavior of $g_n(0)$ as a function of temperature is shown in figure 2 for different values of the binding energy E_b and for both balanced and imbalanced systems. The function $g_n(0)$ diverges when the temperature achieves the limit $T = T_c^*$ at which $\Delta = 0$. This result explicitly follows from the analytic properties of the long-wavelength expansion of the distribution functions as discussed above. The temperature T_p at which $g_n(0) = 0$ lies below the temperature T_c^* where we find that $\Delta = 0$, and above the critical temperature T_{BKT} for superfluidity.

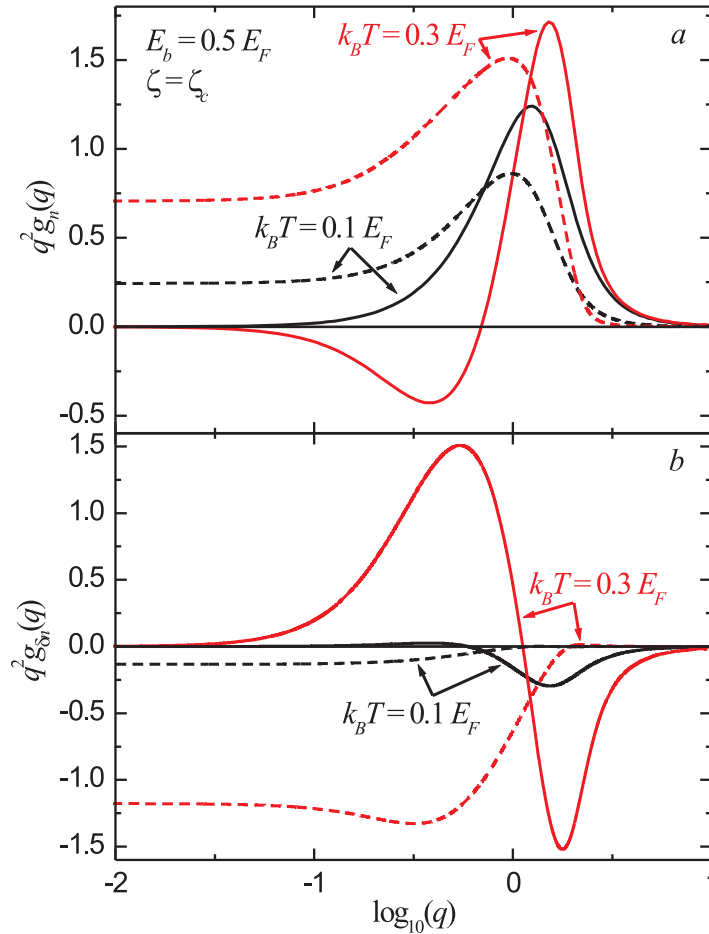


Figure 1. Distribution functions for (a) the fluctuation contribution to the fermion density and (b) the density difference, at the binding energy $E_b = 0.5 E_F$. The solid and dashed curves show the spectral functions obtained, respectively, within the GPF formalism and within the standard NSR scheme. The spectral functions are calculated for critical values $\zeta = \zeta_c$ of the chemical potential imbalance, and for two different temperatures. In the graphs, the spectral functions are multiplied by q^2 in order to clearly show their behavior at small q .

The temperature T_p does not correspond to a phase transition, because the gap equation is satisfied with a finite density both below and above T_p . Nevertheless, because T_p is the temperature at which the fluctuation density of states changes its qualitative behavior, we hypothesize that T_p corresponds to a crossover between the normal and pseudogap states. This will be further substantiated by comparing our spectral functions with the experimental ones in section 5. The joint solution of the gap and number equations within the GPF theory then formally provides a non-superfluid quasicondensate at temperatures below T_p . Indeed, for temperatures $T_{\text{BKT}} < T < T_p$ the phase coherence is destroyed by the phase fluctuations according to the BKT mechanism, resulting in the phase fluctuating quasicondensate discussed by Kagan *et al* [7]. Through the interpretation of the spectral function, we will denote this temperature region as the ‘pseudogap regime’. It is worth noting that the total fermion density

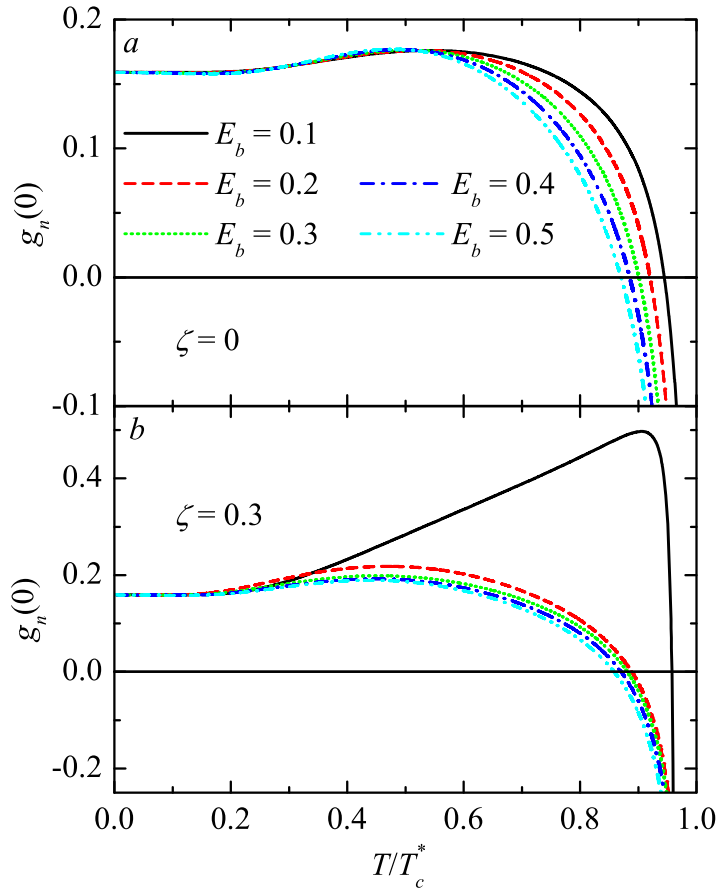


Figure 2. The fluctuation distribution function $g_n(0)$ as a function of temperature for $\zeta = 0$ (a) and $\zeta = 0.3$ (b). The values of the binding energy are shown in the figure.

within the GPF theory is finite at $T = T_p$ without the necessity to introduce any cutoff in the integrals over q . In the next section we set up phase diagrams identifying the regions where the superfluid phase and the non-coherent paired phase occur.

4. Phase diagrams

In order to obtain the complete set of equations for phase diagrams, the number equations (21) and the generalized gap equation (8) are solved jointly with the equation for the BKT transition temperature T_{BKT} determined by [30]

$$T_{\text{BKT}} - \frac{\pi}{2} \rho_s(T_{\text{BKT}}) = 0, \quad (51)$$

where ρ_s is the superfluid pair density given by equation (22). To investigate the phase transitions for the Fermi gas in 2D for different binding energies, we have calculated the critical temperatures of the BKT phase transition T_{BKT} and the critical temperature T_p below which the phase fluctuating quasicondensate is formed, as a function of the binding energy E_b . Because the fluctuation contribution to the density is finite at T_p and at T_{BKT} , these temperatures can be

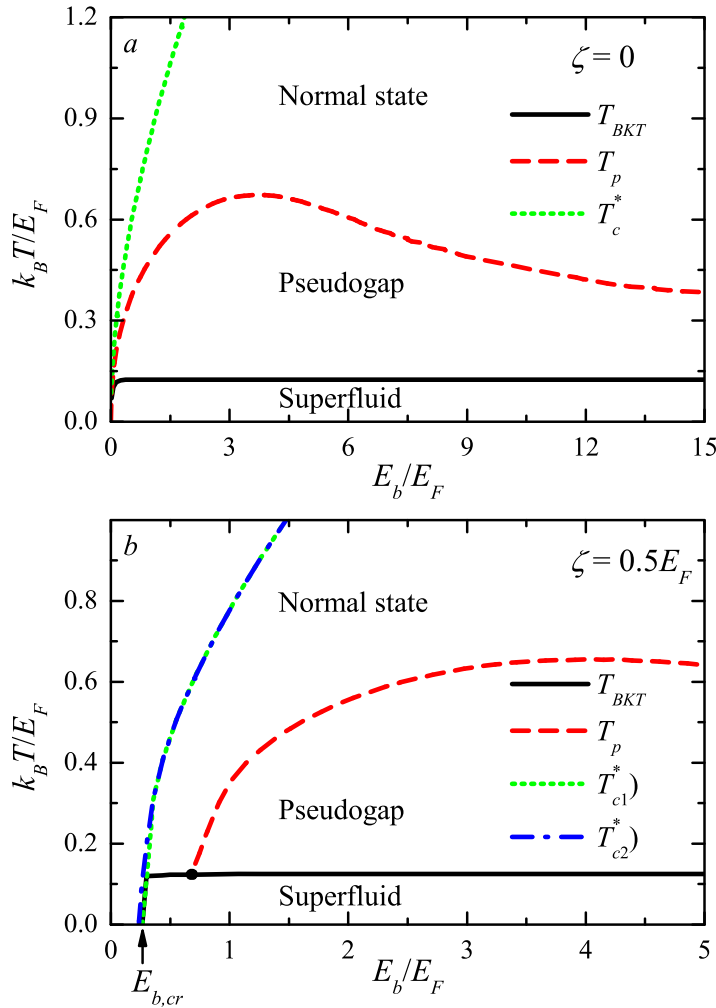


Figure 3. Phase diagrams for the Fermi gas in 2D (a) in the case of equal spin-up and spin-down populations and (b) for the imbalanced Fermi gas with the chemical potential imbalance $\zeta = 0.5$. The crossover pairing temperature T_p for the pseudogap formation and the BKT transition temperature T_{BKT} are shown by dashed and solid curves, respectively. The dot-dashed and dotted curves show the mean-field phase transition temperatures T_{c1}^* , T_{c2}^* (explained in the text). The arrow indicates the lowest binding energy at non-zero imbalance when preformed pairs can arise.

self-consistently determined from the joint solution of the gap and number equations with the *complete* thermodynamic potential $\Omega = \Omega_{sp} + \Omega_{fluct}$.

The phase diagrams in figure 3 show the critical temperatures for cold fermions in 2D as a function of the binding energy E_b for the balanced case (panel (a)) and for the chemical potential imbalance $\zeta = 0.5$ (panel (b)). The formation of the superfluid state is indicated by the critical temperature T_{BKT} of the BKT phase transition. The pseudogap temperature T_p is the upper bound for the existence of the phase fluctuating quasicondensate described in the previous section. We also show the mean-field temperature for pair formation, T_c^* , obtained by solving

gap and number equations with $\Omega = \Omega_{\text{sp}}$. According to [54] (for 3D), the unitary gas can exist in the normal state with pairing correlations called preformed pairs which survive at temperatures up to this T_c^* . The critical temperatures for the balanced case, figure 3(a), were calculated in [55]. Here they are reproduced in order to compare them with those for a non-zero imbalance. The population imbalance brings new features to the phase diagram: a phase separation region (between T_{c1}^* and T_{c2}^*) and a minimum binding energy $E_{b,\text{cr}}$ required for superfluidity.

For the balanced Fermi gas the superfluid state exists for any value of the binding energy: the BKT critical temperature as well as other critical temperatures gradually decrease with decreasing E_b , remaining always finite. However, when $\zeta \neq 0$ a minimum value of the binding energy $E_{b,\text{cr}}$ is required for superfluidity to exist even at $T = 0$. As shown in figure 3, the pseudogap temperature T_p does not grow unboundedly when increasing the binding energy E_b . For $\zeta = 0.5$ it achieves its maximum at around $E_b \approx 4$ and then slowly decreases tending to a finite value. Consequently, in the strong-coupling regime the pseudogap temperature is suppressed with respect to the mean-field prediction, where it is often identified with our pair formation temperature T_c^* , as in [54]. This behavior is qualitatively similar to that for the critical temperature T_c as a function of $1/a_s$ for the cold fermions in 3D obtained first in [2] accounting for the Gaussian fluctuations.

The critical temperatures T_{c1}^* and T_{c2}^* coincide with each other in the balanced case, and they can be different in the imbalanced case: the area between T_{c1}^* and T_{c2}^* is the ‘phase-separated state’. In the phase-separated state, uniform phases are not possible. The temperatures T_{c1}^* and T_{c2}^* have already been calculated in [33]. The temperature T_p is determined for the state with $\Delta \neq 0$. Therefore, a non-zero imbalance does not lead to a splitting of this critical temperature. However, a tricritical point appears at $T_p = T_{\text{BKT}}$ in the phase diagram joining three regions: the superfluid state, the pseudogap regime and the normal state. This tricritical point is rather conventional as far as the pseudogap temperature indicates a crossover rather than a sharp transition.

At zero imbalance, $T_p > T_{\text{BKT}}$, and the phase coherence in the range $T_{\text{BKT}} < T < T_p$ is destroyed by phase fluctuations that lead to a phase fluctuating quasicondensate. However, at non-zero imbalance, there is a region where the pseudogap temperature crosses the BKT temperature for superfluidity. This result is interesting in connection with recent experiments on high- T_c superconductors [56], which show a crossing of the zero-field superconducting transition temperature and the temperature, indicating the opening of the pseudogap in overdoped $\text{La}_{2-x}\text{Sr}_x\text{CuO}_4$. The crossing of pseudogap temperature and BKT temperature is also seen in figure 4, showing the phase diagram in the variables (T, ζ) , for the binding energy $E_b/E_F = 0.04$. Here, the same critical temperatures and phase regions are identified as in figure 3(b). Increasing imbalance is not only detrimental to the superfluid phase, but also suppresses the pseudogap regime.

5. Comparison with experiment

In the experiment [17] on the pairing of cold fermions in two dimensions, the single-particle spectral function $A(\mathbf{q}, \omega)$ is measured for different values of the wave number q . The spectral function exhibits peaks whose positions indicate the energies of the pair excitations. In the strong-coupling regime, these energies are close to the pair binding energy E_b . However, as stated in the paper, some discrepancies remain between the peak positions observed in the experiment and those predicted by the mean-field theory. The deviation ‘could stem from

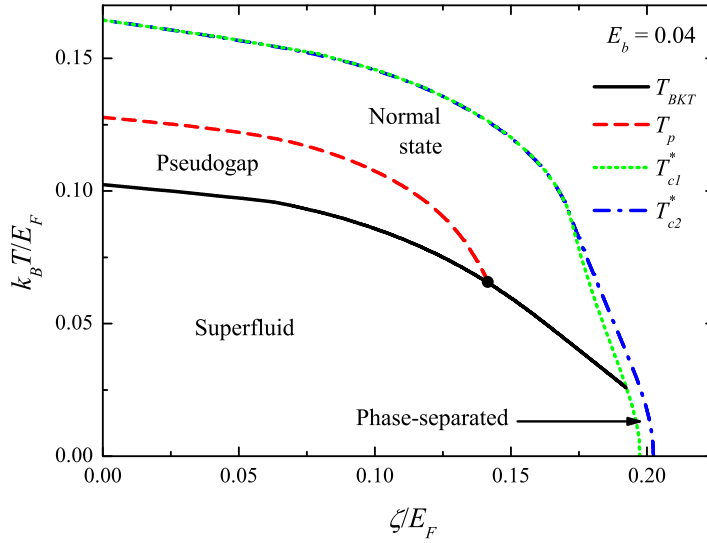


Figure 4. Finite-temperature phase diagram for cold fermions in 2D in the variables (T, ζ) for the binding energy $E_b = 0.04E_F$. The full dot indicates a tricritical point.

beyond mean-field effects provoked by our two-dimensional geometry and interaction energy shifts' [17].

In the GPF approach, the pair fluctuation contribution of the fermion density is expressed by the integral (32), where the structure factor $J(\mathbf{q}, \omega)$ describes the spectrum of pair excitations of the fermion system. Thus there should be correspondence of the peaks of the structure factor $J(\mathbf{q}, \omega)$ with the peaks of the spectral function $A(\mathbf{q}, \omega)$. In this connection, we compare the positions of the peaks of the spectral function measured in [17] with those of the structure factor calculated within the GPF approach. The results are shown in figure 5 for $q = 0$ and $T/T_F = 0.27$, where $k_B T_F \equiv E_F$. The 2D scattering length a_{2D} is related to the binding energy E_b as $a_{2D} = \hbar/\sqrt{mE_b}$. The value of the Fermi wave vector taken from [17] is $k_F = 8.1 \mu\text{m}^{-1}$. When using the mass of the fermion atom $m \approx 39.964 \text{ u}$, we found that the frequency $\nu_F \equiv E_F/(2\pi\hbar)$ corresponding to the Fermi energy is $\nu_F = 8.2967 \text{ kHz}$.

For the visualization of the peaks of the structure factor, we have used $J(\mathbf{q}, \omega + i\gamma)$ with a finite damping parameter γ (as in [38, 39], where this parameter was introduced to facilitate the numeric calculations). Here, the value $\gamma = 0.2\pi/\beta$ is used, where $\beta = 1/(k_B T)$ is the inverse temperature.

The parameters of the state (the chemical potential μ and the gap parameter Δ) are determined for each plot from the joint solution of the gap and number equations. In the number equation, the Gaussian fluctuations are included within the GPF formalism. The GPF method provides a finite (convergent) pair fluctuation contribution for any finite Δ without any cutoff for the pair momentum. This is to be contrasted with the standard NSR scheme, which leads to a divergence of the fluctuation contribution at any Δ . Therefore, the standard NSR scheme cannot be used for the description of the pseudogap state, whereas the GPF approach can describe this regime.

In figure 5, the high peak at $\omega = 0$ in our results has no relation to the energies of the pair excitations: it is an intrinsic feature of the structure factor. The other peak of our structure

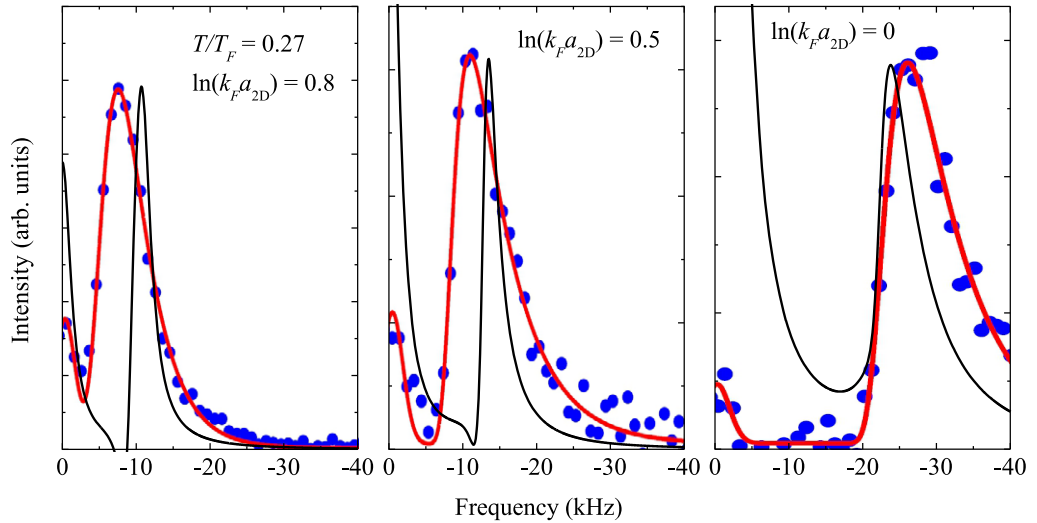


Figure 5. Spectra of pair excitations compared with experimental data. Full dots are the measured energy distribution curve $A(q = 0, \omega)$ for $\ln(k_F a_{2D}) = 0.8$ from [17]. The red solid line is the fit by elementary functions to the experimental data performed in [17]. The black solid line is the structure factor $J(q = 0, \omega)$ calculated in the present work within the GPF approach.

factor at $\omega < 0$ is positioned remarkably close to the measured peak of the spectral function attributed to the pair excitation energy in [17], especially for the relatively high coupling strength at $\ln(k_F a_{2D}) = 0$. A possible reason for the remaining difference between the peak positions of the calculated structure factor $J(\mathbf{q}, \omega)$ and the measured peak spectra is the experimental uncertainty in the determination of the Fermi wave vector, which can be slightly different from the reported value $k_F = 8.1 \mu\text{m}^{-1}$. Another possible source of the remaining difference is the similar experimental uncertainty in $\ln(k_F a_{2D})$. In particular, this uncertainty can be provided by the fact that the Fermi wave vector determined in [17] is a trap-averaged rather than local quantity. It should be noted that the structure factor $J(\mathbf{q}, \omega)$ calculated with the mean-field values for μ and Δ leads to a large discrepancy between the peaks of $J(\mathbf{q}, \omega)$ and those of the measured spectral function. This confirms the importance of including fluctuations through the GPF approach in the description of the pseudogap state of cold fermions in 2D.

In [17], the pairing crossover temperature T^* and the pseudogap pairing temperature $T_B^* < T^*$ have been introduced. The temperature T^* coincides with the mean-field transition temperature T_c^* . The temperature T_B^* , as stated in [17], indicates the formation of pairs, and has the same physical meaning as the temperature T_p obtained in our study. As far as the transition between the normal and paired states is a crossover rather than a true phase transition, the pairing temperatures T_B^* and T_p only approximately indicate the formation of a paired state. In figure 6, the pseudogap pairing temperature T_p is compared with the experimental data for T_B^* . The dotted curve shows the scaled mean-field transition temperature from [17]; the scaling indicates that the experimental result for T_B^* is a factor of 0.36 smaller than the mean-field prediction. We see that, in contrast to the mean-field result, the value of T_p obtained in the present treatment lies in the same range as the experimentally determined temperature T_B^* . This coincidence is worth remarking. However, the conclusions from the latter comparison of two temperatures need care,

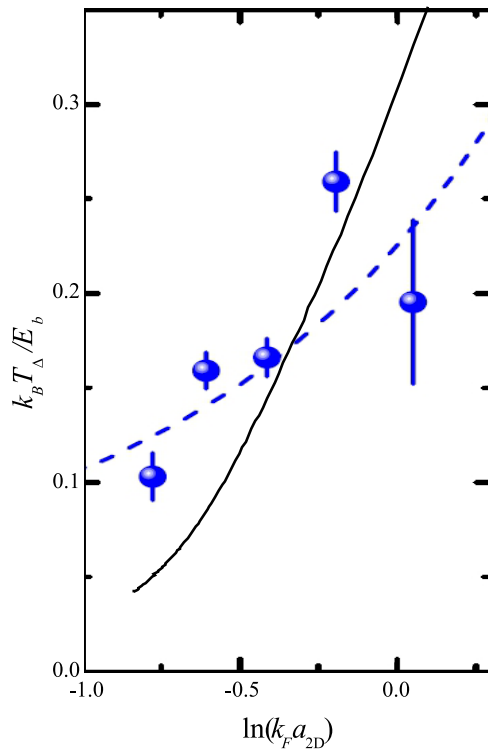


Figure 6. Pseudogap pairing temperature compared with experimental data. Solid curve: the calculated pseudogap pairing temperature T_p (in units of E_b/k_B) compared with the experimentally [17] determined pairing temperature T_B^* (full dots). Dotted curve: the mean-field critical temperature T_c^* scaled by a factor of 0.36.

because the temperature in [17] is measured in the weakly interacting regime and hence it may differ from the actual temperature in the strongly interacting regime.

It is stated in [17] that the discrepancy between the mean-field and experimental pairing temperatures could suggest that the appearance of a back-bending feature in the spectral function [20], which has been interpreted as a signature for many-body pairing, is only qualitative evidence. However, the present results show that the fluctuations can drastically reduce the pairing temperature T_p with respect to T_c^* . Thus there is no discrepancy between experiment and theory when taking into account the fluctuations.

6. Conclusions

The T -matrix approach straightforwardly applied to cold fermions in two dimensions leads to a divergent fermion density for any finite temperature. We have shown in the present work that taking into account the variation of the order parameter in the number equations, as suggested in the GPF approach [13–15], provides a divergence-free description of the paired state in two dimensions. This was shown both through numerical calculations and through an analytic expansion at long wavelengths and low energies, where the divergence occurs in the standard NSR approach. The formalism allows us to study the effects of the fluctuations both at zero

and at finite temperatures, and we find that fluctuations affect the critical binding energy to obtain pairing and superfluidity in the presence of imbalance. Moreover, the formalism also gives access to the density of states of the pair fluctuations, from which we have defined a pseudogap temperature T_p as the temperature where an instability appears in the pair fluctuation density. The pseudogap temperature defined in this way agrees with the measured values of the pseudogap temperature in 2D Fermi gases. Also, the location of the peaks in the spectral functions for pair fluctuations is shown to agree with the experimental observations. The pseudogap temperature T_p , along with the critical temperature T_{BKT} for superfluidity and the pair formation temperature T_c^* , has been calculated as a function of binding energy, temperature and imbalance, from which we obtain the phase diagram as shown in figures 3 and 4. Whereas in the mean field the pseudogap temperature is usually identified with the pair formation temperature, we found that the inclusion of fluctuations beyond the mean field strongly suppresses the pseudogap temperature with respect to the mean-field pair formation temperature. Moreover, in the presence of imbalance, the pseudogap temperature may cross the BKT temperature for superfluidity. The results obtained here in the context of superfluid quantum gases shed new light on the study of the pseudogap phase in layered high-temperature superconductors, where the question of the crossing of the pseudogap temperature with the superconducting temperature, and the presence of preformed pairs, remains an open question.

Acknowledgments

Discussions with M Zwierlein are gratefully acknowledged. This work was supported by FWO-V projects G.0356.06, G.0370.09N, G.0180.09N, G.0365.08, G.0115.12N and G.0119.12N and the WOG WO.033.09N (Belgium). JT acknowledges support from the Special Research Fund of the University of Antwerp under grant no. BOF NOI UA 2004.

References

- [1] Bloch I, Dalibard J and Zwerger W 2008 *Rev. Mod. Phys.* **80** 885
- [2] Sá de Melo C A R, Randeria M and Engelbrecht J R 1993 *Phys. Rev. Lett.* **71** 3202
- [3] Mermin N D and Wagner H 1966 *Phys. Rev. Lett.* **17** 1133
- [4] Hohenberg P C 1967 *Phys. Rev.* **158** 383
- [5] Penrose O and Onsager L 1956 *Phys. Rev.* **104** 576
- [6] Yang C N 1962 *Rev. Mod. Phys.* **34** 694
- [7] Kagan Yu, Svistunov B V and Shlyapnikov G V 1987 *Zh. Eksp. Teor. Fiz.* **93** 552
Kagan Yu, Svistunov B V and Shlyapnikov G V 1987 *Sov. Phys.—JETP* **66** 314 (Engl. transl.)
- [8] Berezinskii V L 1971 *Sov. Phys.—JETP* **32** 493
- [9] Kosterlitz J M and Thouless D J 1973 *J. Phys. C: Solid State Phys.* **6** 1181
Kosterlitz J M 1974 *J. Phys. C: Solid State Phys.* **7** 1046
- [10] Hadzibabic Z, Krüger P, Cheneau M, Battelier B and Dalibard J 2006 *Nature* **441** 1118
- [11] Nozières P and Schmitt-Rink S 1985 *J. Low Temp. Phys.* **59** 195
- [12] Schmitt-Rink S, Varma C M and Ruckenstein A E 1989 *Phys. Rev. Lett.* **63** 445
- [13] Hu H, Liu X-J and Drummond P D 2006 *Europhys. Lett.* **74** 574
- [14] Hu H, Liu X J and Drummond P D 2006 *Phys. Rev. A* **73** 023617
- [15] Hu H, Liu X J and Drummond P D 2010 *New J. Phys.* **12** 063038
- [16] Salasnich L and Toigo F 2011 *J. Low Temp. Phys.* **165** 239
- [17] Feld M, Fröhlich B, Vogt E, Koschorreck M and Köhl M 2011 *Nature* **480** 75

- [18] Sommer A T, Cheuk L W, Ku M J H, Bakr W S and Zwierlein M W 2012 *Phys. Rev. Lett.* **108** 045302
- [19] van der Marel D 2011 *Nature Phys.* **7** 10
- [20] Gaebler J P, Stewart J T, Drake T E, Jin D S, Perali A, Pieri P and Strinati G C 2010 *Nature Phys.* **6** 569
- [21] Perali A, Palestini F, Pieri P, Strinati G C, Stewart J T, Gaebler J P, Drake T E and Jin D S 2011 *Phys. Rev. Lett.* **106** 060402
- [22] Palestini F, Perali A, Pieri P and Strinati G C 2012 *Phys. Rev. B* **85** 024517
- [23] Magierski P, Wlazlowski G and Bulgac A 2011 *Phys. Rev. Lett.* **107** 145304
- [24] Tsuchiya S, Watanabe R and Ohashi Y 2009 *Phys. Rev. A* **80** 033613
- [25] Chen Q, Stajic J, Tan S and Levin K 2005 *Phys. Rep.* **412** 1
- [26] Babaev E and Kleinert H 1999 *Phys. Rev. B* **59** 12083
- [27] Gusynin V P, Loktev V M, Quick R M and Sharapov S G 1998 *Int. J. Mod. Phys. B* **12** 3035
- [28] Gusynin V P, Loktev V M and Sharapov S G 1999 *Zh. Eksp. Teor. Fiz.* **115** 1243
Gusynin V P, Loktev V M and Sharapov S G 1999 *Sov. Phys.—JETP* **88** 685
- [29] Traven S V 1994 *Phys. Rev. Lett.* **73** 3451
- [30] Nelson D R and Kosterlitz J M 1977 *Phys. Rev. Lett.* **39** 1201
- [31] Botelho S S and Sá de Melo C A R 2006 *Phys. Rev. Lett.* **96** 040404
- [32] Popov V N 1983 *Functional Integrals in Quantum Field Theory and Statistical Physics* (Dordrecht: Reidel)
- [33] Tempere J, Klimin S N and Devreese J T 2009 *Phys. Rev. A* **79** 053637
- [34] Andersen J O, Al Khawaja U and Stoof H T C 2002 *Phys. Rev. Lett.* **88** 070407
Al Khawaja U, Andersen J O, Proukakakis N P and Stoof H T C 2002 *Phys. Rev. A* **66** 013615
- [35] Prokof'ev N and Svistunov B 2002 *Phys. Rev. A* **66** 043608
- [36] Randeria M, Duan J-M and Shieh L-Y 1990 *Phys. Rev. B* **41** 327
- [37] Tempere J, Wouters M and Devreese J T 2007 *Phys. Rev. B* **75** 184526
- [38] Tempere J, Klimin S N, Devreese J T and Moshchalkov V V 2008 *Phys. Rev. B* **77** 134502
- [39] Tempere J, Klimin S N and Devreese J T 2008 *Phys. Rev. A* **78** 023626
- [40] He L and Zhuang P 2008 *Phys. Rev. A* **78** 033613
- [41] Zwierlein M W, Schirotzek A, Schunck C H and Ketterle W 2006 *Science* **311** 492
Partridge G B, Li W, Kamar R I, Liao Y-A and Hulet R G 2006 *Science* **311** 503
- [42] Radzihovsky L and Sheehy D E 2010 *Rep. Prog. Phys.* **73** 076501
- [43] Petrov D S and Shlyapnikov G V 2001 *Phys. Rev. A* **64** 012706
- [44] Wouters M and Orso G 2006 *Phys. Rev. A* **73** 012707
- [45] Diener R B, Sensarma R and Randeria M 2008 *Phys. Rev. A* **77** 023626
- [46] Diener R B and Randeria M 2010 *Phys. Rev. A* **81** 033608
- [47] Keeling J, Eastham P R, Szymanska M H and Littlewood P B 2005 *Phys. Rev. B* **72** 115320
- [48] Taylor E, Griffin A, Fukushima N and Ohashi Y 2006 *Phys. Rev. A* **74** 063626
- [49] Ohashi Y and Griffin A 2003 *Phys. Rev. A* **67** 063612
- [50] Fukushima N, Ohashi Y, Taylor E and Griffin A 2007 *Phys. Rev. A* **75** 033609
- [51] Perali A, Pieri P, Pisani L and Strinati G C 2004 *Phys. Rev. Lett.* **92** 220404
- [52] Pieri P, Pisani L and Strinati G C 2005 *Phys. Rev. B* **72** 012506
- [53] Klimin S N, Tempere J and Jeroen Devreese P A 2011 *J. Low Temp. Phys.* **165** 261
- [54] Randeria M 2010 *Nature Phys.* **6** 561
- [55] Klimin S N and Tempere J 2011 *J. Low Temp. Phys.* **162** 291
- [56] Rourke P M C *et al* 2011 *Nature Phys.* **7** 455